Engineering Solid Mechanics 6 (2018) 315-330

Contents lists available at GrowingScience

Engineering Solid Mechanics

homepage: www.GrowingScience.com/esm

# Rock heterogeneity numerical simulation as a factor of drill bit instability

**Tetiana Pryhorovska**[a*]

[a]*Ivano-Frankivsk National Technical University of Oil and Gas, Ivano-Frankivsk, Ukraine*

**ARTICLEINFO**

*Article history*:
Received 10 June, 2018
Accepted 26 August 2018
Available online
26 August 2018

*Keywords*:
*Rock cutting*
*Rock granulometric composition*
*PDC cutter*
*Static force balance*
*Rock reaction force*

**ABSTRACT**

Heterogeneity is an important factor controlling fracture initiation, accumulation, and propagation within rock destruction. Traditionally, rock reaction instability within rock destruction is associated with rock non-homogeneity or considered self-excited, but no clear relations between rock structure options and reaction force oscillation were proposes. This work hypothesizes the idea rock structure options are one of the factors of drill bit whirling. The authors innovated the Wojtanowicz and Kuru's force static balance model to numerically simulate 3-cutter movement in a rock space, assuming a crack propagates by rock grains getting around. Instability of deviation between directions of cutting force and crack propagation causes rock reaction instability. Novelty of this work is to consider the mutual influence of rock granulomentric composition options (sizes, shape and distribution of grains) and drill bit design options (cutter diameter, distance between adjacent cutters, etc.) on rock reaction force oscillation. The follow tendencies were observed: rock grain dimension increasing and grain concentration increasing were accompanied with rock reaction force magnitude decreasing; random grain placing and/or grain random dimensions caused increasing of rock reaction force scattering; random grain sizes are more essential for rock reaction forces (and their projections) scattering than random grain distribution.



## 1. Introduction

Rock heterogeneity is an important factor controlling fracture initiation, accumulation, and propagation within rock destruction. Internal spatial variability in terms of mineralogy, grain sizes and anisotropy affects the yielding process (Villeneuve et al. 2012). Rock reaction instability within rock destruction is associated with non-homogeneity or considered self-excited (Richard et al. 2001), but no clear relations between material homogeneity characteristics and rock reaction force oscillations were proposed. In the frame of drilling, rock reaction force instability is a cause of drill bit whirling. Traditionally, this process is assumed as chaotic, and rock reaction force oscillations are simulated by random functions (Spanos et al., 2002, Depouhon & Detournay 2014). Simanjuntak and coworkers (2014) studied the effect of rock mass anisotropy on stresses and deformations of tunnels during excavation process. Some researchers have also employed numerical simulations for investigating the fracture process of rocks and concerts (Zhu et al. 2002; Ju et al. 2014). On the other hand, since rock cutting is basically a process of cracking in the rock masses, the fracture toughness of rock that has been investigated in many research studies (Guo et al., 1993, Aliha & Ayatollahi, 2014; Ayatollahi & Aliha, 2007; Aliha et al., 2012, 2013, 2008, 2017; Akbardoost et al., 2014; Aliha & Bahmani, 2017;

* Corresponding author.
E-mail addresses: pryhorovska@gmail.com (T. Pryhorovska)


doi: 10.5267/j.esm.2018.8.002

Jin et al., 2011; Dai et al., 2015; Wei et al., 2016a,b; Razavi et al., 2017; Mirsayar et al., 2016, 2018; Ingraffea, 1982; Fakhri et al., 2017; Lim et al., 1994; Al-shayea, 2005; Zipf & Bieniawski, 1990; Dehghany et al., 2017) can provide useful data for designing rock cutters and drill bits.

The study proposed herein considers the "rock-PDC cutter interaction" problem as a part of the general problem of cutting simulation. There are many "rock-cutter" interaction models, which focus on the rock destruction aspects. Rock cutting models are based on force balancing, and derive from models of metal destruction (Merchant, 1945; Evans & Pomeroy, 1966, Nishimatsu, 1972). These models were developed only for sharp cutters, but the Wojtanowicz and Kuru's model (1993) assumed that a certain worn area has been already formed. However, traditionally, the static balance models used only the general options of rock resistance (rock resistance for pressing, rock crushing resistance, etc.).

The author innovated the Wojtanowicz and Kuru's force static balance model (1993), assuming a crack propagates by rock grains getting around, so rock granulometric composition specifies the deviation angle between directions of cutting force application and crack propagation. Instability of the deviation angle between directions of cutting force and crack propagation causes rock reaction force instability.

The model of cutting force balance assumes the follows:

- two types of "rock-cutter" contact: rock crushing by the cutter's front surface and rock pressing by the cutter's lateral surface; this way, two types of friction forces are considered: the frictional force, acting on the front surface and the friction force acting on the lateral surface, respectively;
- rock reaction force direction is assumed not orthogonal to the cutter's contact surface, but parallel to the crack propagation direction;
- the crack propagates by rock grains getting around, so rock granulometric composition specifies the deviation angle between directions of cutting force and crack propagation.

The first assumption is based on the fact that the real contact surface of the new cutter consists of two plots: the plot on the frontal surface and the plot on the lateral surface (Fig. 1).

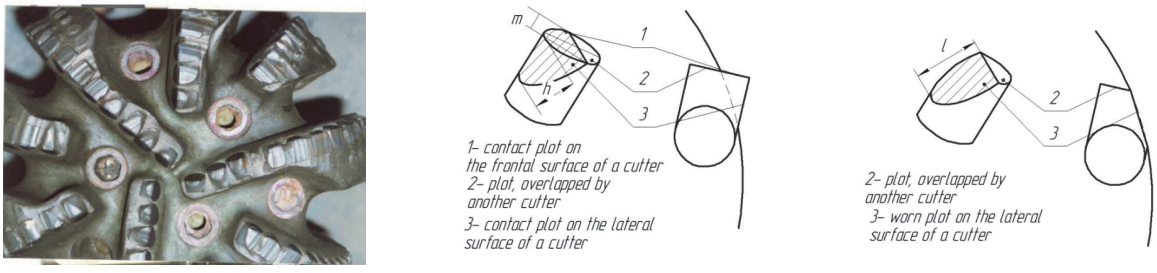


A B C

Fig. 1. Worn PDC drill bits (A) and contact surfaces of the new cutter (B) and the worn one (C): h -height of the lateral contact surface (lateral side of the new cutter); m - width of the frontal contact surface (face of the new cutter); l- length of the lateral contact surface (lateral side of the worn cutter).

Dimensions of contact plots on the frontal and lateral surfaces are defined by the cutter relative position among other cutters. Usually, because of cutters overlapping, only the small part of a PDC plate is used for rock cutting, so sometimes cutter's frontal contact plot dimension is smaller than its lateral contact plot. Proposed herein model assumes commensurate values of frictional forces, generated on these plots, considering dimensions of these plots and difference between the "polycrystalline diamond cutter- rock" and "PDC stud metal-rock" friction coefficients.

The assumption of difference between directions of cutting force and rock reaction force makes possible consideration of rock heterogeneity. In the frame of this work, grain placement and their dimensions specify the heterogeneity options. Wojtanovich and Kuru's model (1993) considers rock propagation direction is similar to the cutting force direction. The author hypothesizes the idea the crack propagates by rock grains getting around, so rock granulometric composition specifies the deviation between directions of cutting force and crack propagation. It means that angle between directions of rock propagation and cutting force is changeable because of circle movement of the cutter. In its turn, rock reaction force, in general, is not stable for all cutter movement length. This hypothesis can explain more oscillation of rock reaction force for the cutter circle movement, than for the cutter linear movement.

In the mentioned above order, this paper puts forward an idea of deviation between directions of cutting force and the crack propagation is an extremely significant factor and affects rock reaction force magnitude. This way, it hypothesizes the idea that rock reaction force changes, and is synchronized with rock component transition within cutting. This work purpose is analyzing a relation between rock reaction forces and rock granulometric composition, which specifies the deviation between directions of cutting force and crack propagation.

## 2. The model of cutter force balancing

A force balance system is developed to represent the forces, acting on the new and worn cutters, as schematically shown in Fig. 2. They are: $P$ - loading (directed at the $P_X; P_Y; P_Z$ angles to the coordinate axes, refer to the placement of the cutter); $Fw$ -contact force, acting on the lateral surface and directed perpendicular to this surface); $R$ - rock reaction force (directed at the $R_X; R_Y; R_Z$ angles to the coordinate axes, refer to the rock heterogeneity direction); $F_T$ -frictional force (acting on the contact surface of the cutter and directed at the $P_X; P_Y; P_Z$ angles to the coordinate axes), $F_T$*-and frictional force (acting on the lateral surface of the cutter and directed along this surface). The subscript "$i$" refers the number of the cutter, placed on the "$j$" blade.

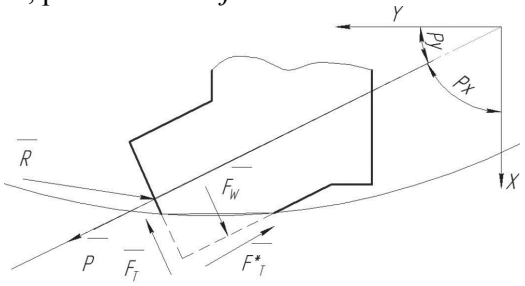


**Fig. 2.** Scheme of forces application.

The model proposed herein derived from the Wojtanowich and Kuru's (1993) model. The vector equation constituted the force balance is:

$$\overline{R}+\overline{P}+\overline{F_T}+\overline{F_T}^{*}+\overline{Fw}=0 \tag{1}$$

The systems of 3-axes projections are the follow:
- for the new cutter:

$$\begin{cases} RX^D = P_{ij}\cdot\cos P_{Xij} - F_{Tij}{}^{*}\cdot\cos P_{Xij} - F_{Tij}\cdot\sin P_{Xij} - F_{Wij}\cdot\sin R_{Xij} \\ RY^D = P_{ij}\cdot\cos P_{Yij} - F_{Tij}{}^{*}\cdot\cos P_{Yij} - F_{Tij}\cdot\sin P_{Yij} - F_{Wij}\cdot\sin R_{Yij} \\ RZ^D = P_{ij}\cdot\cos P_{Zij} - F_{Tij}{}^{*}\cdot\cos P_{Zij} - F_{Tij}\cdot\sin P_{Zij} - F_{Wij}\cdot\sin R_{Zij} \end{cases} \tag{2}$$

- for the worn cutter:

$$\begin{cases} RX_{ij}^{\ D} = -F_W \cdot \sin R_{X\,ij} \\ RY_{ij}^{\ D} = -F_{Tij} * -F_{W\,ij} \cdot \sin R_{Y\,ij} \\ RZ_{ij}^{\ D} = -F_{Tij} * \cdot \cos P_{Zij} - F_{W\,ij} \cdot \sin R_{Z\,ij} \end{cases} \tag{3}$$

Index “D” means the forces are deviated from the coordinate axes. The real direction of rock reaction force and its components depends on the rock heterogeneity. It is manifested in the rock reaction force deviation from the cutting force application direction. In the frame of this work, the author assumes the crack propagates by rock grains getting around. The components of rock reaction force are directed according to the $R_X$ ; $R_Y$ ; $R_Z$ angles to the coordinate axes, similar to the rock heterogeneity direction. It means that in real conditions the X-component of rock reaction force is deviated from the X-axe at the $R_X$-angle, the Y-component of the rock reaction force is deviated from the Y-axe at the $R_Y$-angle and the Z-component of rock reaction force is deviated from the Z-axe at the $R_Z$-angle, respectively. The scheme of force direction and deviation is presented in Fig.3.

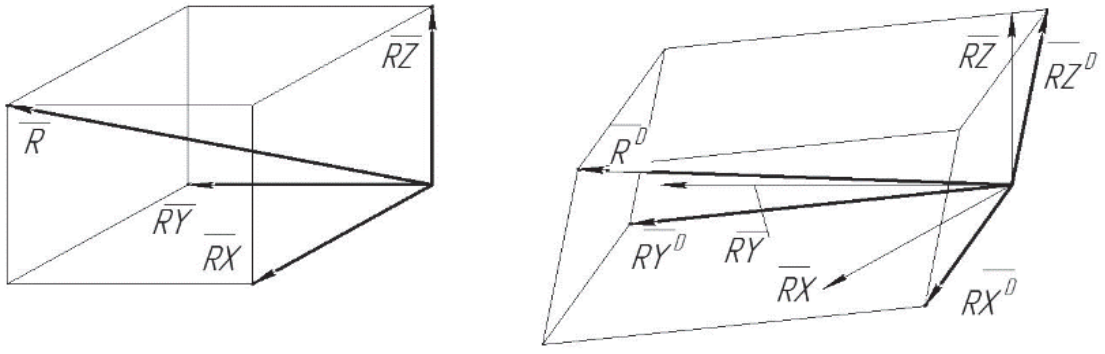


A B

**Fig. 3.** The scheme of rock reaction force components deviation (A- Rock reaction force components without deviation, B - Rock reaction force components with deviation).

The total rock reaction force is defined as:

$$R = \sqrt{RX^2 + RY^2 + RZ^2} \tag{4}$$

In the frame of this work, the authors assumed values of rock reaction forces are similar both for heterogeneity consideration and non-consideration $|R| = |R^D|$, but their directions are differ. Components of total rock reaction force considered not orthogonal, contrary to the X,Y,Z projections of the non-deviated rock reaction force. In their turns, components of the deviated total rock reaction refer its X,Y,Z-projections as follows:

$$RX^D = RX \cdot \cos R_X,\ RY^{\ D} = RY \cdot \cos R_Z,\ RZ^{\ D} = RZ \cdot \cos R_Z \tag{5}$$

This way, the most effective rock destruction case is the co-direction of loading application and cracks propagation: $\angle(P_{Xij}) = \angle(R_{Xij})$, $\angle(P_{Yij}) = \angle(R_{Yij})$ and $\angle(P_{Zij}) = \angle(R_{Zij})$.

The next stage is definition of the frictional forces. According to the assumption of two types of frictional forces, one can make the following substitutions for the frictional forces definition:

- $F_T$ - frictional force, acting on the contact surface of the cutter

$$F_{Tij} = S_{1ij} \cdot \sigma \cdot f_{1ij}, \tag{6}$$

where $S_{1ij}$ - area of the frontal contact surface (the face of the cutter), $f_{1ij}$-" polycrystalline diamond - rock" friction coefficient, $\sigma$ - rock crushing resistance.

- $F_T$ *- frictional force, acting on the lateral cutter surface of the cutter:

$$F_{Tij}^* = S_{2ij}^* \cdot f_{2ij}^* \cdot \sigma^*, \tag{7}$$

where $S_{2ij}$ *- area of the lateral contact surface of the cutter, $f_{2ij}$ *-" PDC stud metal - rock" friction coefficient, $\sigma^*$ - rock resistance for pressing.

This approach makes possible considering contact conditions for both areas (materials of the PDC plate and PDC stud, rock crushing and rock pressing for the frontal and lateral plots of the cutter respectively, etc.).

In general, the force balance equation systems Eq. (2) and Eq. (3) become as follows:

-for the new cutter:

$$\begin{cases} RX_{ij}^{D} \cos R_X = P_{ij} \cdot \cos P_{Xij} - S_{2ij}^* \cdot f_{2ij}^* \cdot \sigma^* \cdot \cos P_{Xij} - \\ - S_{1ij} \cdot \sigma \cdot f_{1ij} \cdot \sin P_{Xij} - S_{2ij}^* \cdot \sigma^* \cdot \sin R_X \\ RY_{ij}^{D} \cos R_Y = P_{ij} \cdot \cos P_{Yij} - S_{2ij}^* \cdot f_{2ij}^* \cdot \sigma^* \cdot \cos P_{Yij} - \\ - S_{1ij} \cdot \sigma \cdot f_{1ij} \cdot \sin P_{Yij} - S_{2ij}^* \cdot \sigma^* \cdot \sin R_Y \\ RZ_{ij}^{D} \cos R_Z = P_{ij} \cdot \cos P_{Zij} - S_{2ij}^* \cdot f_{2ij}^* \cdot \sigma^* \cdot \cos P_{Zij} - \\ - S_{1ij} \cdot \sigma \cdot f_{1ij} \cdot \sin P_{Zij} - S_{2ij}^* \cdot \sigma^* \cdot \sin R_Z \end{cases} \tag{8}$$

for the worn cutter:

$$\begin{cases} RX_{ij}^{D} = -F_W \cdot \sin R_{X\,ij} \\ RY_{ij}^{D} = -F_{Tij}^* - F_{W\,ij} \cdot \sin R_{Y\,ij} \\ RZ_{ij}^{D} = -F_{Tij}^* \cdot \cos P_{Zij} - F_{W\,ij} \cdot \sin R_{Z\,ij} \end{cases} \tag{9}$$

## 3. Numerical simulation of total rock reaction force depending on rock heterogeneity

The purpose of the numerical simulation is definition of the total reaction force for 3 cylindrical cutters (13 mm diameter) installed into the PDC drill bit blade related to the grain sizes and grain concentrations as the rock options. The PDC blade movement was defined as a set of the cutters placement points. Total cutting depth was 15 mm per one blade rotation, 72 analyzed points refer to 2 full round path for every cutter. The study was conducted for the new cutters moved with constant velocity. Options of the cutter sizes and their placement are presented in Table 1. The scheme of simulation is presented in Fig.4.

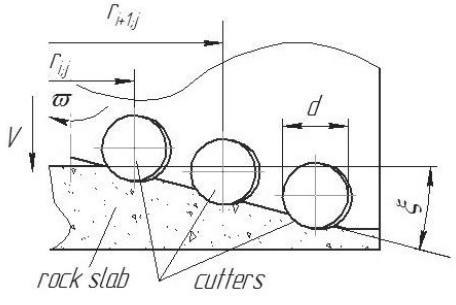


**Fig. 4.** The simulation scheme.

**Table 1.** Options of cutter sizes and their placement according to the simulation scheme

| Cutter | Angle of the cutter inclination to the OX axis *Px, deg* | Horizontal distance to the drill bit axis | Initial coordinate of cutting force application in the rock slab, mm | | |
|---|---|---|---|---|---|
| | | | X | Y | Z |
| 1 | 10 | 11 mm | 10.142 | 0 | 2.7175 |
| 2 | 10 | 28 mm | 25.597 | 0.01 | 6.858 |
| 3 | 10 | 45 mm | 34.777 | 0 | 9.317 |

To simulate the rock cutting, the author has used MathCad. Grains into the simulated rock slab were distributed uniformly and randomly. For all simulations, the follow options were calculated:

- grain center coordinates for all rock slab;
- cutting force application coordinates for all cutters throughout cutter movements;
- distances from cutting forces applications for all cutters to all grain centers throughout the cutters movement;
- the grain, providing the minimal distance to the cutting forces application point for each cutter, its position and relative coordinate;
- position and relative coordinate in the rock slab of the grain, with minimal distance to the cutting forces application point for each cutter;
- direction and inclination options of the crack propagation vectors for all cutters throughout the cutter movements;
- Rock reaction forces and their coordinate axe projections for all cutters throughout cutters movements.

The scheme of grain package is presented in Fig.5.

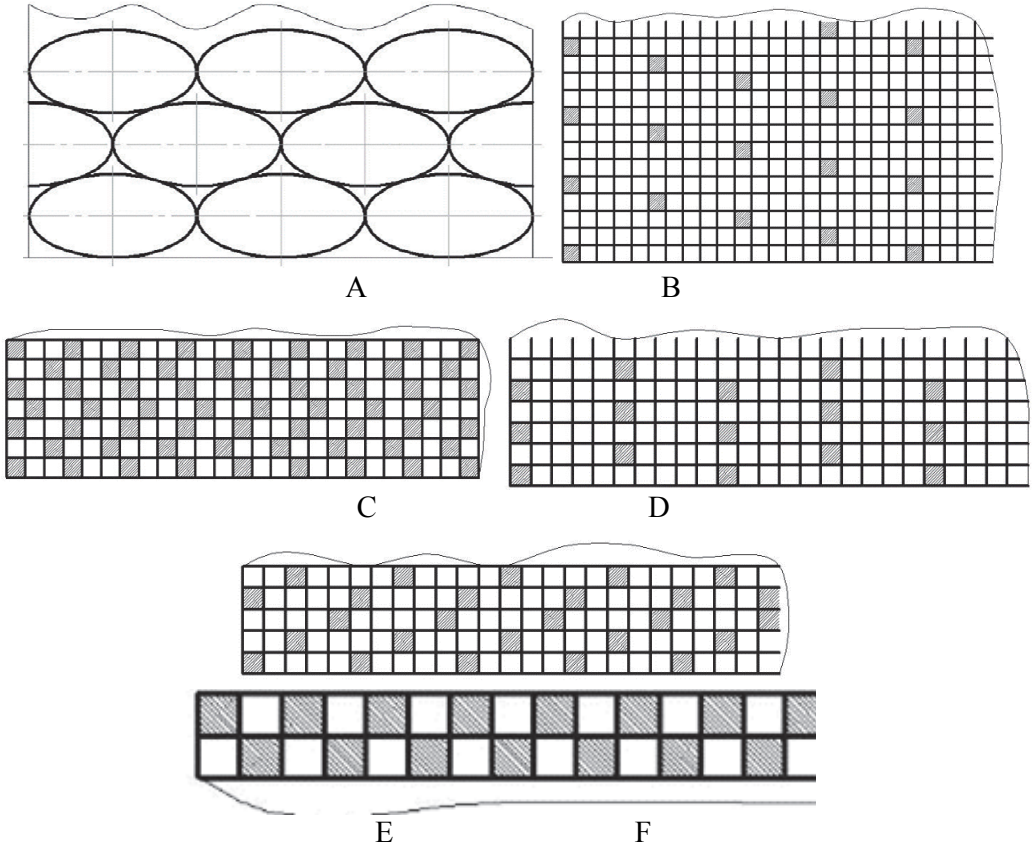


**Fig. 5.** The grain package scheme: A-simulations 1-4; B- simulation 5; C-simulation 6; D- simulation 7; E-simulation 8; F-simulation 9

The study has the follow stages:

- study on total rock reaction forces (and their projections) related to the grain sizes with grain continuous placement (simulations 1-4);
- study on total rock reaction forces (and their projections) related to the grain concentration with grain uniform placement and their constant sizes (simulations 5-9);
- study on total rock reaction forces (and their projections) related to the grain concentrations with grain random placement and their constant sizes (simulations 10-14);
- study on total rock reaction forces (and their projections) related to the grain concentrations with grain random placement and their random sizes (simulations 15-19).

*3.1 Total cutting forces numerical simulations related to the grain sizes with grain continuous placement*

The simulations were provided for 4 types of tightly packed ellipsoidal grains (sizes are presented in Table 2). The grain package scheme is presented in Fig. 5.

**Table 2.** Ellipsoidal grains sizes, m

| Semi-axis length | Simulation 1 | Simulation 2 | Simulation 3 | Simulation 4 |
|---|---|---|---|---|
| a | 0.001 | 0.006 | 0.03 | 0.04 |
| b | 0.0005 | 0.003 | 0.015 | 0.02 |
| c | 0.0025 | 0.0015 | 0.0075 | 0.01 |

Fig. 6-9 depict rock reaction forces and their projections for every cutter for the simulations 1-4.

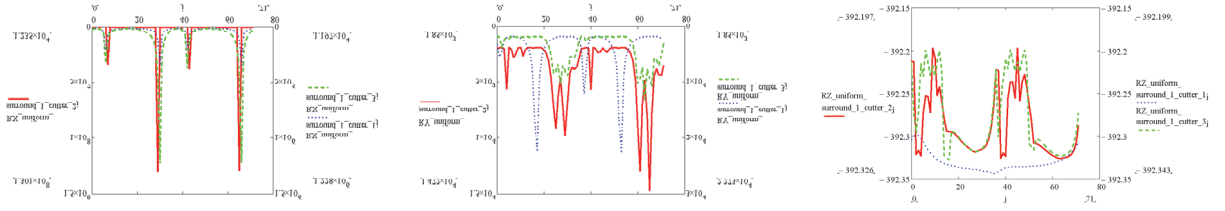

**Fig. 6.** Rock reaction force projections for the simulation 1: continuous grains distribution, ellipsoidal grains (a=0.001m, b=0.0005m, c=0.00025m

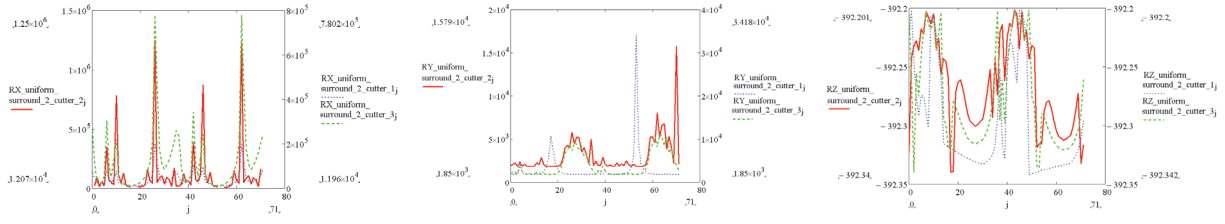

**Fig. 7.** Rock reaction force projections for the simulation 2: continuous grain distribution, ellipsoidal grains (a=0.001m, b=0.0005m, c=0.00025m)

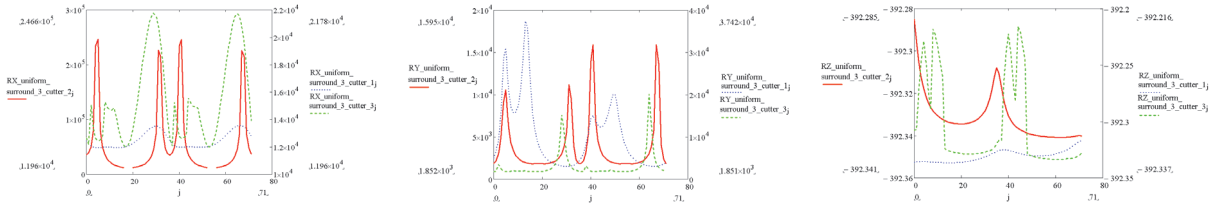

**Fig. 8.** Rock reaction force projections for the simulation 3: continuous grain distribution, ellipsoidal grains (a=0.001m, b=0.0005m, c=0.00025m)

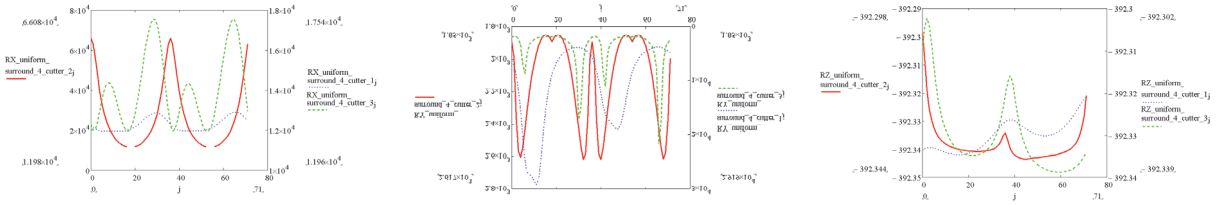

**Fig. 9.** Rock reaction force projections for the simulation 4: continuous grain distribution, ellipsoidal grains (a=0.001m, b=0.0005m, c=0.00025m)

The general tendencies were observed:

- average values of rock reaction forces (unlike their projections) were close for all simulations and did not depend on grain sizes and their concentrations;
- all force (and their projections) patterns were chaotic without obvious trends and/or periodicity, but had irregular peaks; no statistically significant regularity of the rock reaction force projections for the 1, 2 and 3 cutters were observed for all simulations;
- values of the X-projections of rock reaction forces were essentially bigger, than the Y-projection and Z-projection. For all simulations the X-projection values exceeded the Y- projection values in 10-12 times and exceeded the Z- projection values in 30-35 times;
- values of the X-projections of the rock reaction forces were essentially bigger, than the Y-projections and Z-projections. For all simulations the X-projection values exceeded the Y-projection values in 10-12 times and exceeded Z- projection values in 30-35 times;
- the most scattered data were values of the X-projections; the lowest scattering of the Z-projection values made possible their peak values neglecting; peak values of the X-projection exceeded average ones in 10000 -12000 times, the Y-projection- in 8-10 times;
- grain size increasing was accompanied with peak number decreasing for all rock reaction force projections; grain size increasing was accompanied with chaotic decreasing and partial periodicity of the Z-projection of the rock reaction force.

*3.2 Total rock reaction forces related on grain concentration with grain uniform placement and their constant sizes.*

Simulations were provided for 5 types of grain concentrations: 5%, 10%, 20%, 30% and 50% (Fig. 5). The ellipsoidal grains with semi-axes length a=0.004, b=0.002, c=0.001 m were uniformly distributed into the rock mass slab. Fig.10-14 depict rock reaction forces (and their projections) related on the grain sizes with the grain continuous placement (simulations 5-9) for the blade with 3 cutters.

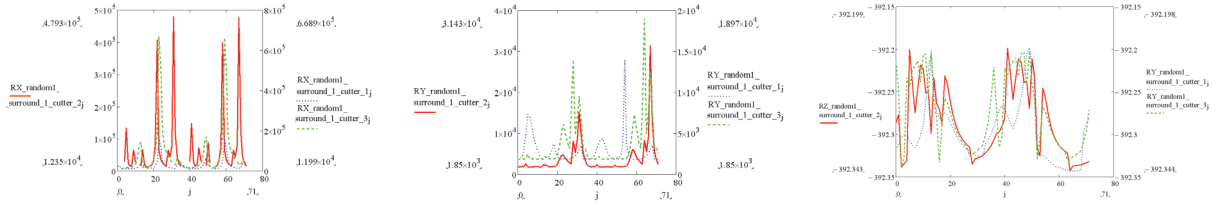

**Fig. 10.** Rock reaction force projections for the simulation 5: uniform grains distribution, ellipsoidal grains (a=0.001m, b=0.0005m, c=0.00025m), grain concentration 5%.

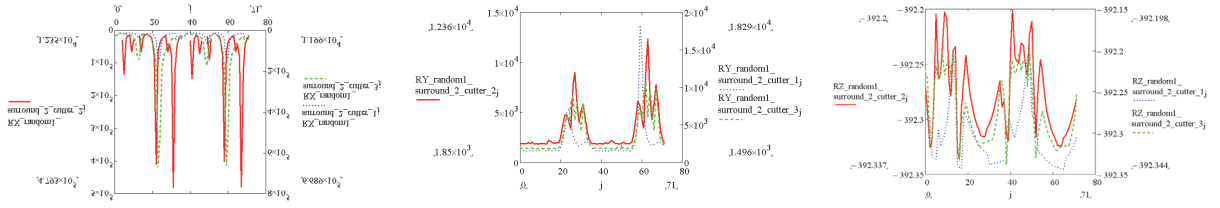

**Fig. 11.** Rock reaction force projections for the simulation 6: uniform grain distribution, ellipsoidal grains (a=0.001m, b=0.0005m, c=0.00025m), grain concentration 10%

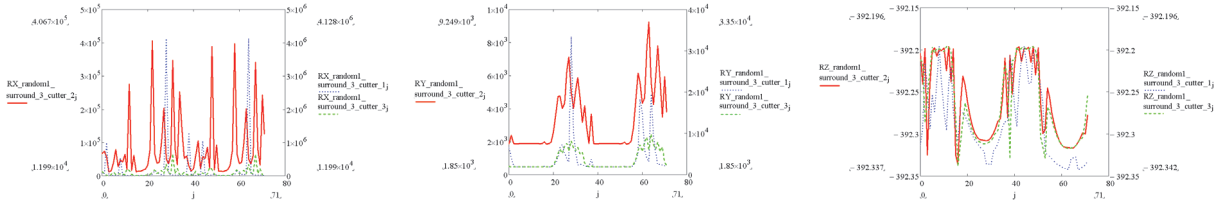

**Fig. 12.** Rock reaction force projections for the simulation 7: uniform grain distribution, ellipsoidal grains (a=0.001m, b=0.0005m, c=0.00025m), grain concentration 20%

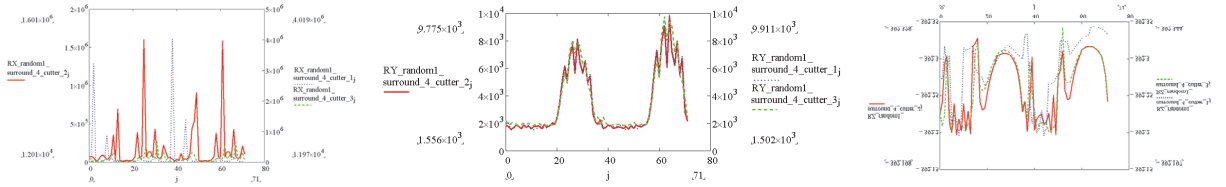

**Fig. 13.** Rock reaction force projections for the simulation 8: uniform grains distribution, ellipsoidal grains (a=0.001m, b=0.0005m, c=0.00025m), grain concentration 30%

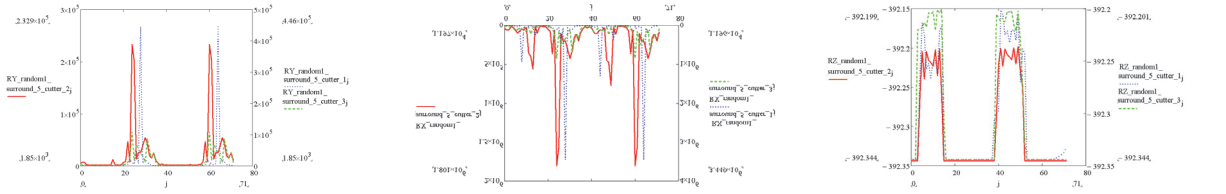

**Fig. 14.** Rock reaction force projections for the simulation 9: uniform grains distribution, ellipsoidal grains (a=0.001m, b=0.0005m, c=0.00025m), grain concentration 50%.

The general tendencies were observed:

- average values of the rock reaction forces (unlike their projections) were close for all simulations;
- all force (and their projections) patterns were chaotic without obvious trends and/or periodicity, but had irregular peaks;
- no statistically significant regularity of the rock reaction force projections for the 1, 2 and 3 cutters were observed for all simulations;
- values of the X-projection of the rock reaction forces were essentially bigger, than the Y-projections and Z-projections. For all simulations the X-projection values exceeded the Y-projection values in 10-12 times and exceeded the Z- projection values in 30-35 times;
- the most scattered data were values of the Z-projection; the lowest scattering of the Z-projection data made possible their peak values neglecting;
- peak values of X-projection exceeded average in 10000 -12000 times, Y-projection- in 8-10 times;
- grain concentration increasing was accompanied with periodicity of partial the Y-projection and decreasing of Z and X projections chaotic;
- grain concentration increasing was accompanied with peak values decreasing and ratio “peak values/average value” decreasing for the Y and Z projections (except 50% concentration);
- the maximal X-projection value scattering was observed for the 20% grain concentration.
- no periodicity was observed for the X-projections;
- grain concentration increasing was accompanied with peak number increasing for the X projection.
- XY- projection patterns had gaps. Patterns of the total rock reaction forces and their horizontal projections had gaps, which can explain extremes in the rock reaction forces within drill bit whirling.

### *3.3 Total rock reaction forces (and their projections) related on grain concentration with their random placement and constant/random sizes*

The study aimed at comparing values of the total rock reaction forces (and their projections) for grain uniform and random distributions. Besides, there were two cases of random grain distribution: constant sized and random sized grains. Fig.15-19 depict the rock reaction forces (and their projections)

related on grain sizes with their random placement (simulations 10-14) for the blade with 3 cutters. Fig.20-24 depict the rock reaction forces (and their projections) related on random grain sizes with their random placement (simulations 15-19) for the blade with 3 cutters.

Simulations were provided for 5 types of grain concentrations: 5%, 10%, 20%, 30% and 50% for the ellipsoidal grains (semi-axes length a=0.004, b=0.002, c=0.001 m) and random sized grains.

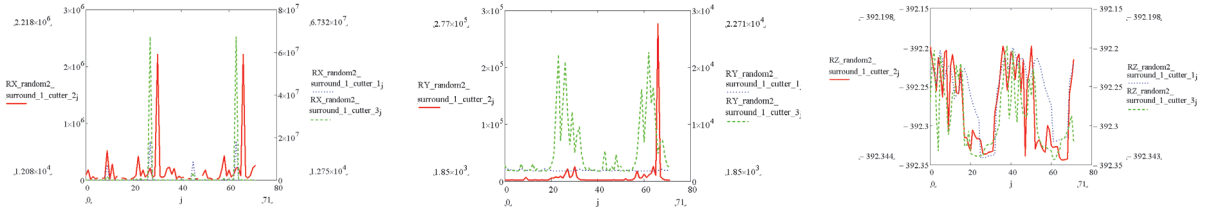

**Fig.15.** Rock reaction force projections for the simulation 10: random grain distribution, ellipsoidal grains (a=0.001m, b=0.0005m, c=0.00025m), grain concentration 5%

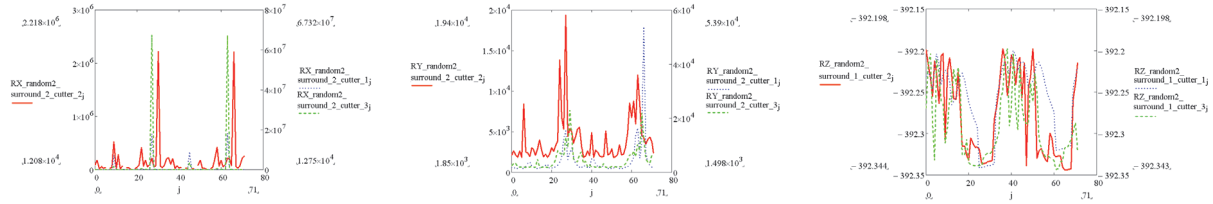

**Fig. 16.** Rock reaction force projections for the simulation 11: random grain distribution, ellipsoidal grains (a=0.001m, b=0.0005m, c=0.00025m), grain concentration 10%

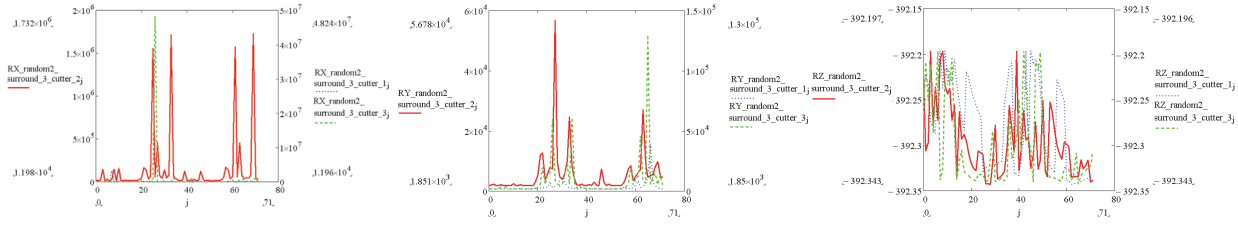

**Fig. 17.** Rock reaction force projections for the simulation 12: random grains distribution, ellipsoidal grains (a=0.001m, b=0.0005m, c=0.00025m), grain concentration 20%

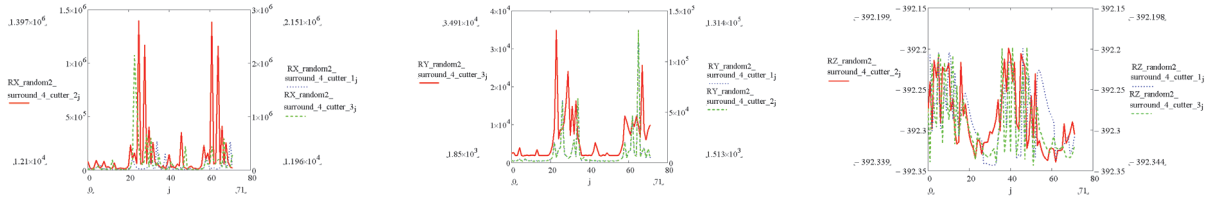

**Fig. 18.** Rock reaction force projections for the simulation 13: random grains distribution, ellipsoidal grains (a=0.001m, b=0.0005m, c=0.00025m), grain concentration 30%

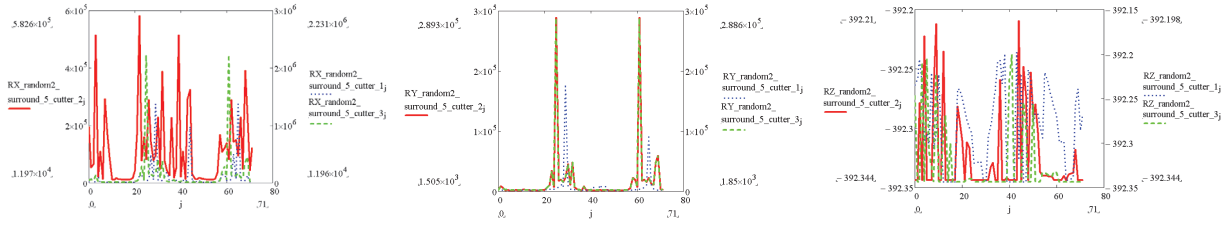

**Fig. 19.** Rock reaction force projections for the simulation 13: random grain distribution, ellipsoidal grains (a=0.001m, b=0.0005m, c=0.00025m), grain concentration 50%

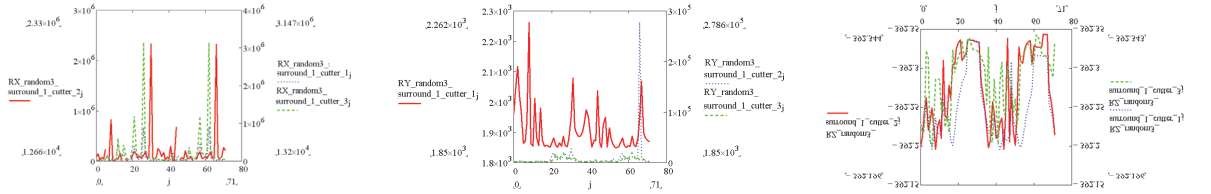

**Fig. 20.** Rock reaction force projections for the simulation 15: random grain distribution, random sized grains, grain concentration 5%

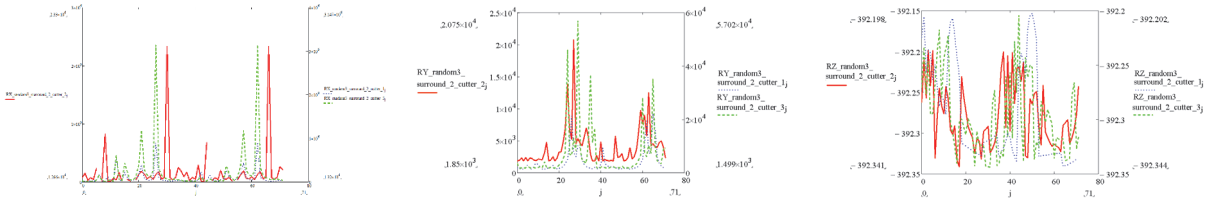

**Fig. 21.** Rock reaction force projections for the simulation 16: random grains distribution, random sized grains, grain concentration 15%

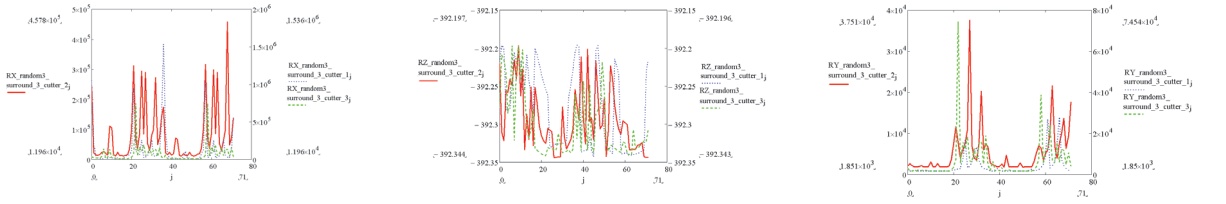

**Fig. 22.** Rock reaction force projections for the simulation 17: random grains distribution, random sized grains, grain concentration 20%

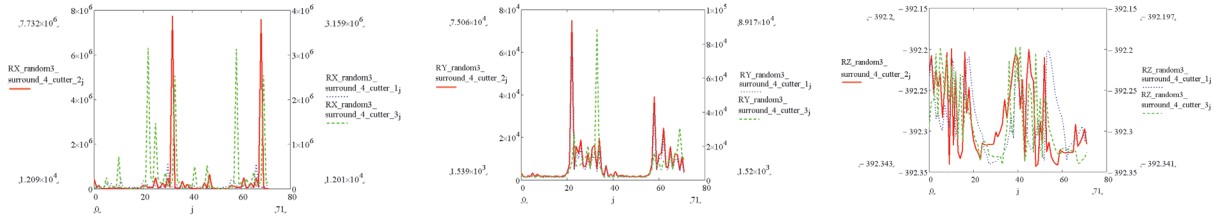

**Fig. 23.** Rock reaction force projections for the simulation 18: random grains distribution, random sized grains, grain concentration 30%

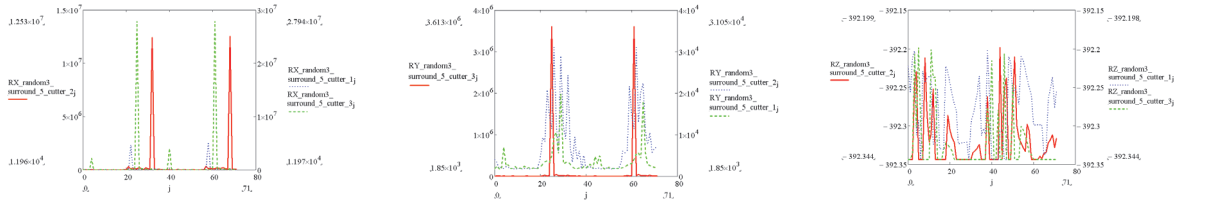

**Fig. 24.** Rock reaction force projections for the simulation 19: random grain distribution, random sized grains, grain concentration 50%

The follow tendencies were observed:

**5% grain concentration:**

- The X and Y projection values were close (deviation no more than 10-15%) for the random and uniform grain distribution. The X and Y projection patterns of random distributed random sized grains were essentially differing than patterns for the random and uniform distributed ellipsoidal grains for all 3 cutters simulations.

- The biggest number of the Z projection peaks was observed for random distributed random sized grain patters, the smallest – for the uniform distributed ellipsoidal grain pattern;
- The patterns of the Z projection values for the random distributed ellipsoidal grains were close to the random distributed random sized grain patterns; but essentially differ for the uniform distributed ellipsoidal grain patterns.
- The Z-projection patterns for the random and uniform grain distributions were essentially differ for all 3 cutters.

**10% grain concentration:**

- The patterns of the X and Z projections for the random and uniform grain distributions were close for all 3 cutters;
- The biggest numbers of the Y projection peaks were observed for the random distributed random sized grain patterns, the smallest – for the uniform distributed ellipsoidal grain patterns;
- The biggest data scattering was observed for the random distributed random sized grain patters, the smallest – for the uniform distributed ellipsoidal grain patterns.

**20% grain concentration:**

- The patterns of the X and Z projections had no essential difference for the uniform and random grain distributions;
- The biggest numbers of the X,Y,Z projection peaks and data scattering were observed for the random distributed random sized grain patterns, the smallest – for the uniform distributed ellipsoidal grain patterns;

**30% grain concentration:**

- The patterns of the X and Y projections for the random distributed random sized grains had the biggest ratio of the "peak/average" values;
- The patterns of the Z projections for the random distributed ellipsoidal and random sized grains had no significant differences for all 3 cutters;

**50% concentration:**

- for all projections the biggest ratio of "peak/average" values were observed for the random distributed random sized grain cases;
- The patterns of the Z projections for the random distributed ellipsoidal and random sized grains had no significant differences for all 3 cutters;

The general tendencies for all simulations were observed:

- All patterns had were chaotic, had no obvious trends and periodicity, but had irregular peaks;
- the most scattered data were values of the X-projection; the lowest scattering of the Z-projection data made possible their peak value neglecting;
- grain concentration increasing was associated with the "peak/average" ratio decreasing for all simulations;
- grain concentration increasing was associated with the decreasing of grain random sizes influence on the force projection scattering.

## 4. Conclusion

Rock destruction is associated with rock reaction force instability, which is the cause of drill bit whirling. Traditionally, this process is assumed as a chaotic, and rock reaction force oscillations are simulated by random functions. This article focuses on the problem of rock reaction force instability

depending on rock granulometric composition. Based on the Wojtanowicz and Kuru's force balancing model, it considers two types of the "rock-cutter" contact: the rock crushing by the face of the cutter and the rock pressing by the lateral surface of the cutter. This contact areas generate 2 types of frictional forces.

Besides, proposed herein force balancing model assumes the crack propagates by rock grains getting around, so rock granulometric composition specifies the deviation angle between directions of cutting force and crack propagation. It considers the deviation between directions of cutting force and crack propagation is an extremely significant factor and affects rock reaction force magnitude. This way it hypothesizes an idea the changes in rock reaction force values synchronized with the rock components transition during cutting.

The numerical simulations were conducted for 2 full circle movements of the 3 cylindrical cutters installed into the PDC drill bit blade. The rock slabs were simulated as the sets of grains with different sizes and placing. The study was conducted for the new cutters only, which moved with constant velocity.

The follow general tendencies were observed:

- average values of the total forces were close, but their current projections were distributed randomly;
- all force (and their projection) patterns were chaotic without obvious trends and/or periodicity, but had irregular peaks;
- no statistically significant regularity of rock reaction force projections for 1, 2 and 3 cutters were observed for all simulations;
- values of the X-projection of rock reaction forces were essentially bigger, than the Y-projections and Z-projections;
- the biggest scattering was observed for the X-projection; the lowest scattering of the Z-projection data made possible their peak values neglecting;
- grain increasing did not caused changes for rock reaction force projection minimal and average values, but caused maximal peak value decreasing.
- grain concentration increasing was accompanied with the peak values decreasing, the ratio "peak values/average value" decreasing for the Y and Z projection and peak number decreasing;
- the random placing and/or random sizes of the grains caused increasing of the rock reaction force scattering;
- random grain size is the more essential factor of the rock reaction force (and its projections) scattering then the random grain distribution.

In the frame of the rock destruction simulations, the author can conclude, rock heterogeneity is one of the factors of rock reaction force oscillations. Rock grain dimension increasing and grain concentration increasing were accompanied with the rock reaction force magnitude decreasing; the random grain placing and/or grain random dimensions caused increasing of the rock reaction force scattering; random grain sizes are more essential for rock reaction forces (and their projections) scattering than random grain distribution. The random structure options of rock can explain random values of the rock reaction force and do not consider rock destruction as a self-excited and/or random process.

## Acknowledgments

The authors are grateful for all the collective of Ivano-Frankivsk National University of Oil and Gas (Ukraine) and for sharing their pearls of wisdom of this research, and thanks the anonymous reviewers for their so-called insights.

## References

Akbardoost, J., Ayatollahi, M. R., Aliha, M. R. M., Pavier, M. J., & Smith, D. J. (2014). Size-dependent fracture behavior of Guiting limestone under mixed mode loading. *International Journal of Rock Mechanics and Mining Sciences*, *71*, 369-380.

Al-Shayea, N. A. (2005). Crack propagation trajectories for rocks under mixed mode I–II fracture. *Engineering Geology*, *81*(1), 84-97.

Aliha, M. R. M., & Ayatollahi, M. R. (2014). Rock fracture toughness study using cracked chevron notched Brazilian disc specimen under pure modes I and II loading–A statistical approach. *Theoretical and Applied Fracture Mechanics*, *69*, 17-25.

Aliha, M. R. M., & Bahmani, A. (2017). Rock fracture toughness study under mixed mode I/III loading. *Rock Mechanics and Rock Engineering*, *50*(7), 1739-1751.

Aliha, M. R. M., Ayatollahi, M. R., & Akbardoost, J. (2012). Typical upper bound–lower bound mixed mode fracture resistance envelopes for rock material. *Rock Mechanics and Rock Engineering*, *45*(1), 65-74.

Aliha, M. R. M., Ayatollahi, M. R., & Pakzad, R. (2008). Brittle fracture analysis using a ring-shape specimen containing two angled cracks. *International Journal of Fracture*, *153*(1), 63.

Aliha, M. R. M., Berto, F., Mousavi, A., & Razavi, S. M. J. (2017). On the applicability of ASED criterion for predicting mixed mode I+ II fracture toughness results of a rock material. *Theoretical and Applied Fracture Mechanics*, *92*, 198-204.

Aliha, M. R. M., Hosseinpour, G. R., & Ayatollahi, M. R. (2013). Application of cracked triangular specimen subjected to three-point bending for investigating fracture behavior of rock materials. *Rock mechanics and rock engineering*, *46*(5), 1023-1034.

Aliha, M. R. M., Mahdavi, E., & Ayatollahi, M. R. (2017). The influence of specimen type on tensile fracture toughness of rock materials. *Pure and Applied Geophysics*, *174*(3), 1237-1253.

Ayatollahi, M. R., & Aliha, M. R. M. (2007). Fracture toughness study for a brittle rock subjected to mixed mode I/II loading. *International Journal of Rock Mechanics and Mining Sciences*, *44*(4), 617-624.

Ayatollahi, M. R., & Aliha, M. R. M. (2008). On the use of Brazilian disc specimen for calculating mixed mode I–II fracture toughness of rock materials. *Engineering Fracture Mechanics*, *75*(16), 4631-4641.

Dai, F., Wei, M. D., Xu, N. W., Ma, Y., & Yang, D. S. (2015). Numerical assessment of the progressive rock fracture mechanism of cracked chevron notched Brazilian disc specimens. *Rock Mechanics and Rock Engineering*, *48*(2), 463-479.

Dehghany, M., Saeidi Googarchin, H., & Aliha, M. R. M. (2017). The role of first non-singular stress terms in mixed mode brittle fracture of V-notched components: an experimental study. *Fatigue & Fracture of Engineering Materials & Structures*, *40*(4), 623-641.

Depouhon, A., & Detournay, E. (2014). Instability regimes and self-excited vibrations in deep drilling systems. *Journal of Sound and Vibration*, *333*(7), 2019-2039.

Evans, I., & Pomeroy, C. D. (1966). *The strength, fracture and workability of coal*. Pergamon.

Fakhri, M., Amoosoltani, E., & Aliha, M. R. M. (2017). Crack behavior analysis of roller compacted concrete mixtures containing reclaimed asphalt pavement and crumb rubber. *Engineering Fracture Mechanics*, *180*, 43-59.

Guo, H., Aziz, N. I., & Schmidt, L. C. (1993). Rock fracture-toughness determination by the Brazilian test. *Engineering Geology*, *33*(3), 177-188.

Ingraffea, A. R. (1981, January). Mixed-mode fracture initiation in Indiana limestone and Westerly granite. In *The 22nd US Symposium on Rock Mechanics (USRMS)*. American Rock Mechanics Association.

Jin, Y., Yuan, J., Chen, M., Chen, K. P., Lu, Y., & Wang, H. (2011). Determination of rock fracture toughness K IIC and its relationship with tensile strength. *Rock Mechanics and Rock Engineering*, *44*(5), 621.

Ju, P., Wang, Z., Zhai, Y., Su, D., Zhang, Y., & Cao, Z. (2014). Numerical simulation study on the optimization design of the crown shape of PDC drill bit. *Journal of Petroleum Exploration and Production Technology*, *4*(4), 343-350.

Lim, I. L., Johnston, I. W., Choi, S. K., & Boland, J. N. (1994, June). Fracture testing of a soft rock with semi-circular specimens under three-point bending. Part 2—mixed-mode. In *International journal of rock mechanics and mining sciences & geomechanics abstracts* (Vol. 31, No. 3, pp. 199-212). Pergamon.

Merchant, M. E. (1945). Mechanics of the metal cutting process. I. Orthogonal cutting and a type 2 chip. *Journal of Applied Physics*, *16*(5), 267-275.

Mirsayar, M. M., Berto, F., Aliha, M. R. M., & Park, P. (2016). Strain-based criteria for mixed-mode fracture of polycrystalline graphite. *Engineering Fracture Mechanics*, *156*, 114-123.

Mirsayar, M. M., Razmi, A., Aliha, M. R. M., & Berto, F. (2018). EMTSN criterion for evaluating mixed mode I/II crack propagation in rock materials. *Engineering Fracture Mechanics*, *190*, 186-197.

Nishimatsu, Y. (1972, March). The mechanics of rock cutting. In *International Journal of Rock Mechanics and Mining Sciences & Geomechanics Abstracts* (Vol. 9, No. 2, pp. 261-270). Pergamon.

Razavi, S. M. J., Aliha, M. R. M., & Berto, F. (2017). Application of an average strain energy density criterion to obtain the mixed mode fracture load of granite rock tested with the cracked asymmetric four-point bend specimens. *Theoretical and Applied Fracture Mechanics*.

Richard, T., Germay, C., & Detournay, E. (2001). *Self-excited stick-slip oscillations of drag bits* (Doctoral dissertation, University of Minnesota).

Simanjuntak, T. D. Y. F., Marence, M., Mynett, A. E., & Schleiss, A. J. (2014). Effect of rock mass anisotropy on deformations and stresses around tunnels during excavation. In *Proceedings of the International Symposium on Dams in Global Environmental Challenges, Bali, Indonesia. pp. II-129–II-136*.

Spanos, P. D., Chevallier, A. M., & Politis, N. P. (2002). Nonlinear stochastic drill-string vibrations. *Journal of Vibration and Acoustics*, *124*(4), 512-518.

Villeneuve, M. C., Diederichs, M. S., & Kaiser, P. K. (2011). Effects of grain scale heterogeneity on rock strength and the chipping process. *International Journal of Geomechanics*, *12*(6), 632-647.

Wei, M. D., Dai, F., Xu, N. W., Liu, J. F., & Xu, Y. (2016b). Experimental and numerical study on the cracked chevron notched semi-circular bend method for characterizing the mode I fracture toughness of rocks. *Rock Mechanics and Rock Engineering*, *49*(5), 1595-1609.

Wei, M. D., Dai, F., Xu, N. W., Zhao, T., & Xia, K. W. (2016a). Experimental and numerical study on the fracture process zone and fracture toughness determination for ISRM-suggested semi-circular bend rock specimen. *Engineering Fracture Mechanics*, *154*, 43-56.

Wojtanowicz, A. K., & Kuru, E. (1993). Mathematical modeling of PDC bit drilling process based on a single-cutter mechanics. *Journal of Energy Resources Technology*, *115*(4), 247-256.

Zhu, W. C., & Tang, C. A. (2002). Numerical simulation on shear fracture process of concrete using mesoscopic mechanical model. *Construction and Building Materials*, *16*(8), 453-463.

Zipf Jr, R. K., & Bieniawski, Z. T. (1990, December). Mixed-mode fracture toughness testing of coal. In *International Journal of Rock Mechanics and Mining Sciences & Geomechanics Abstracts* (Vol. 27, No. 6, pp. 479-493). Pergamon.